ACS APPLIED MATERIALS & INTERFACES

RESEARCH ARTICLE

www.acsami.org

Investigation of Ionic Conductivity and Long-Term Stability of a LiI and KI Coupled Diphenylamine Quasi-Solid-State Dye-Sensitized Solar Cell

S. Agarwala, C. K. N. Peh, and G. W. Ho*

Department of Electrical and Computer Engineering, National University of Singapore, 4 Engineering Drive, Singapore 117576

ABSTRACT: In this work, enhancement of ionic conductivity and long-term stability through the addition of diphenylamine (DPA) in poly(ethylene oxide) (PEO) is demonstrated. Potassium iodide (KI) is adopted as the crystal growth inhibitor, and DPA is used as a charge transport enhancer in the electrolyte. The modified electrolyte is used with titanium dioxide (TiO_2) nanoparticles, which is systematically tuned to obtain high surface area. The dye-sensitized solar cell (DSSC) showed a photocurrent of ~14 $mAcm^2$ with a total conversion efficiency of 5.8% under one sun irradiation. DPA enhances the interaction of the TiO_2 nanoparticle film and the I^-/I_3^- electrolyte leading to high ionic conductivity (~3.5×10^{-3} Scm^{-1}), without compromising on the electrochemical and mechanical stability. Electrochemical impedance spectroscopy (EIS) studies show that electron transport and electron lifetime are enhanced in the DPA added electrolyte due to reduced sublimation of iodine. The most promising feature of the electrolyte is increased device stability with 89% of the overall efficiency preserved even after 40 days.

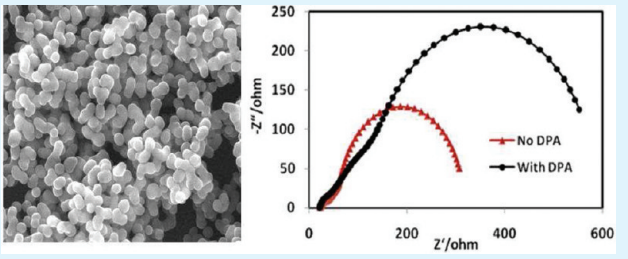

KEYWORDS: quasi-solid-electrolyte, dye-sensitized solar cell, titanium dioxide, nanoparticle

1. INTRODUCTION

Author: Please verify that the changes made to improve the English still retain your original meaning.Depleting fossil fuels and climate changes have sparked intense interest in solar energy harvesting. The focus of the research community is to fabricate high efficiency photovoltaic cells from low cost and environmental friendly semiconductors. One of the key ingredients of DSSC is the electrolyte, which provides the internal electrical conductivity. At present, acetonitrile based liquid electrolytes are commonly used. The use of liquid electrolytes, however, demands perfect sealing of the device to avoid leakage and evaporation of the solvents. Also, current electrolytes suffer from poor stability due to a decrease of tri-iodide concentration through the sublimation of iodine. Both of these issues affect the long-term stability and performance of the liquid electrolyte.

Thus, much work has been done to replace the liquid electrolytes with all-solid-state organic hole-transport materials,[1,2] *p*-type inorganic semiconductors (CuI, CuSCN),[3,4] plastic crystal electrolytes,[5] polymer electrolytes,[6−8] gel electrolytes,[9,10] and less volatile ionic liquids.[11,12] Among the many alternatives, PEO polymer based electrolytes have attracted widespread interest after Ren et al.[13] used them in quasi-solid-state DSSC and reported an efficiency of 3.6%. The repeating units (−CH_2−CH_2−O−) in PEO present a favorable arrangement for the effective interaction of the free electron pair on the oxygen with metal cation. This happens because PEO chains are arranged in a helical conformation with a cavity, which creates an ideal distance for oxygen−cation interaction. Pure PEO electrolytes are chemically stable but suffer from low ionic conductivity (~8.4×10^{-5} Scm^{-1}).[14] The problems associated with the use of pure PEO polymer electrolytes arise from low ionic diffusion which resulted in low penetration of the polymer inside a nanostructured photoanode. This increases the interfacial charge-transfer resistance between the electrode and the electrolyte. The ionic conductivity of these electrolytes is based on segmental motion combined with strong Lewis-type acid−base interactions between the cation and the donor atoms. Higher ionic mobility is prevalent in the amorphous polymer matrix rather than in the crystalline state. Work from several groups have shown that electrolyte stability can be increased either through gelation of the ionic liquid electrolyte or by addition of phenothiazine, which in turn reduces the sublimation of iodine.[15−18]

The aim of this work is to systematically investigate the enhancement of ionic conductivity and long-term stability of PEO based electrolytes with DPA in a TiO_2 nanoparticle photoanode. The ionic conductivity of the PEO based polymer electrolyte is enhanced by incorporating two types of ions (Li^+ and K^+), which aim to decrease the crystallization of the PEO matrix through polymer chain separation. DPA is added to the polymer electrolyte to reduce sublimation of iodine by forming an interactive bond. Finally, this filler free PEO based electrolyte is implemented on TiO_2 nanoparticles which are tuned to obtain high surface area. Stability tests are carried out on the DSSC to ascertain the effectiveness of the new electrolyte system.

2. EXPERIMENTAL SECTION

2.1. Materials. Titanium(IV) isopropoxide, PEO (M_w ~200,000), DPA, lithium iodide (LiI), potassium iodide (KI), iodine (I_2), nitric acid,

Received: March 8, 2011
Accepted: June 7, 2011
Published: June 07, 2011

and acetonitrile were purchased from Sigma-Aldrich. All of the reagents used were of analytical purity. The N719 dye and sealing binder Surlyn were obtained from Solaronix (Switzerland). Fluorine doped tin oxide (FTO) substrates (resistivity 20 Ωsq^{-1}, 16 mm × 22 mm × 1.1 mm) were purchased from Asahi Glass Electronics Pte. Ltd.

2.2. Synthesis of TiO_2 Nanoparticles. Grätzel's method[2] was used to prepare TiO_2 nanoparticles. One milliliter of 0.1 M nitric acid was added to titanium(IV) isopropoxide under constant stirring, and the resulting solution was heated to 90 °C for 8 h. The mixture was cooled down to room temperature and filtered. The filtrate was heated in an autoclave at 240 °C for 12 h. The solution was then dried at room temperature and converted into powder. Different samples with varying amounts of titanium(IV) isopropoxide were prepared.

2.3. Electrolyte Preparation. The polymer electrolyte was prepared by adding 0.264 g of PEO, 0.1 g of LiI, and 0.019 g of I_2 in 50 mL of acetonitrile under continuous stirring. 14.5 wt % of KI was then added. A total of five electrolyte solutions were made with DPA content varying from 0.002 to 0.01 g. The electrolytes were stirred continuously overnight. All of the electrolytes were heated (∼70 °C) to evaporate the solvent. The final product had a gel-like character.

2.4. Solar Cell Assembly. TiO_2 powder was converted into a fine paste using deionized (DI) water without any binder and then spread on FTO glass by the Doctor Blade technique[19] (cell area 0.25 cm^2). One layer of Scotch tape (∼40 μm) was used for all of the electrodes. The films were allowed to dry in ambient conditions before heating at 450 °C for 30 min in air. The films were immersed in an ethanolic solution containing 0.3 mM Ru-dye, *cis*-dithiocyanate-*N*,*N*′-bis(4-carboxylate-4-tetrabutylammoniumcarboxylate-2,2′-bipyridine) ruthenium(II) (known as N719), for 24 h at room temperature. Subsequently, the films were rinsed with ethanol. The electrolyte was injected through a hole in the platinum-coated counter electrode. The hole was then sealed with hot-melt Surlyn film.

2.5. Analysis Techniques. The morphology of synthesized TiO_2 films was examined with a JEOL-2100 high-resolution transmission electron microscope (TEM) with an accelerating voltage of 200 kV and a JEOL FEG JSM 6700 F field-emission scanning electron microscope (FESEM) operating at 10 kV. Film thickness was determined with an Ambios Technology XP 200 profilometer. Structural characterization of the morphology was obtained by X-ray diffraction (XRD) on a Philips X-ray diffractometer with CuKα radiation. Brunauer−Emmett−Teller (BET) measurements were conducted using a Quantachrome Nova 1200 with N_2 as the adsorbate at liquid nitrogen temperature. Photoluminescence (PL) was measured using Accent Rapid Photoluminescence Mapping (RPM 2000) with a He−Cd laser. The photocurrent−voltage of the samples were measured with a solar simulator (Newport 91160A) equipped with an AM filter and a 150 W Xe lamp as the light source. The solar cells were tested at 25 °C with a sourcemeter (Keithley 2420) using Newport IV test station software. The light intensity corresponding to AM 1.5 (100 mW cm^{-2}) was calibrated using a standard silicon solar cell (Oriel, SRC-1000-TC). Incident photon-to-collected-electron conversion efficiency (IPCE) spectra were measured with a spectral resolution of 5 nm using a 300 W xenon lamp and a grating monochromator equipped with order sorting filters (Newport/Oriel). The incident photon flux was determined using a calibrated silicon photodiode (Newport/Oriel). Control of the monochromator and recording of photocurrent spectra were performed using TRACQ Basic software (Newport). Electrochemical impedance spectroscopy (EIS) was recorded with a potentiostat PGSTAT 302N (Autolab, Eco Chemie, The Netherlands) under an illumination of 100 mW cm^{-2}. The frequency range was varied from 0.05 Hz to 100 kHz, and the magnitude of the alternating signal was 10 mV. The conductivity of the electrolyte system was derived from the complex impedance measurements.

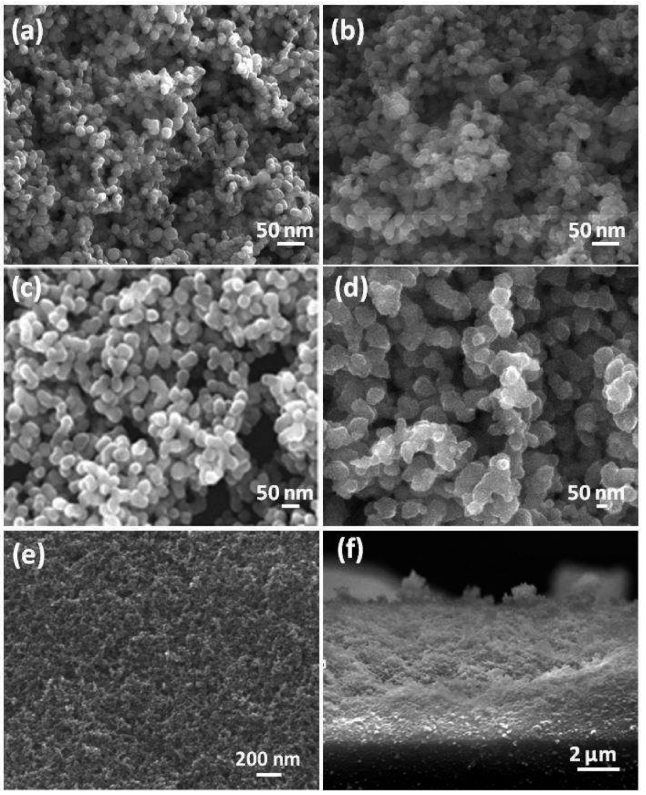

Figure 1. SEM images of films using (a) 30, (b) 40, (c) 50, and (d) 60 mL of titanium isopropoxide. (e) Top and (f) cross-sectional SEM of the film using 30 mL of titanium isopropoxide solution of TiO_2 nanoparticles after calcination at 450 °C for 30 min.

3. RESULTS AND DISCUSSION

3.1. Characterization of TiO_2 Nanoparticles. The FESEM images of TiO_2 nanoparticles prepared using different volumes of titanium isopropoxide are shown in Figure 1. The uniformity and geometry of the TiO_2 nanoparticles can be easily tuned via the amount of titanium isopropoxide added. At a concentration of <30 mL of titanium isopropoxide, TiO_2 nanoparticles are not well-formed. This is due to the low concentration of titanium precursor present. At 30 mL of titanium isopropoxide, nanoparticles with diameters of ∼20−30 nm are formed (Figure 1a). The nanoparticles are relatively well dispersed but are irregularly shaped due to agglomeration. At higher concentrations of 40, 50, and 60 mL of titanium isopropoxide, the diameters of the TiO_2 nanoparticles increase to ∼30, 50, and 150 nm, respectively. Higher extent of agglomeration of the nanoparticles occurs as the precursor concentration is further increased, which results in a large disparity of nanoparticle geometry. Thus, in the subsequent fabrication of the photoanode for DSSC, 30 mL of titanium isopropoxide is used. Figure 1e and f show the planar and cross-sectional views of the doctor bladed film using 30 mL of titanium isopropoxide. The top view of the FESEM images depicts uniform coverage of TiO_2 nanoparticles on the FTO substrate. The TiO_2 nanoparticle film is homogeneous with no observable cracks and adheres well to the FTO. After the calcinations of the nanoparticles at 450 °C, the morphology of the synthesized nanoparticles with 30 mL of titanium isopropoxide is studied using TEM (Figure 2a, b, and c). The TEM images reveal some degree of nanoparticle agglomeration, yet the primary nanoparticles

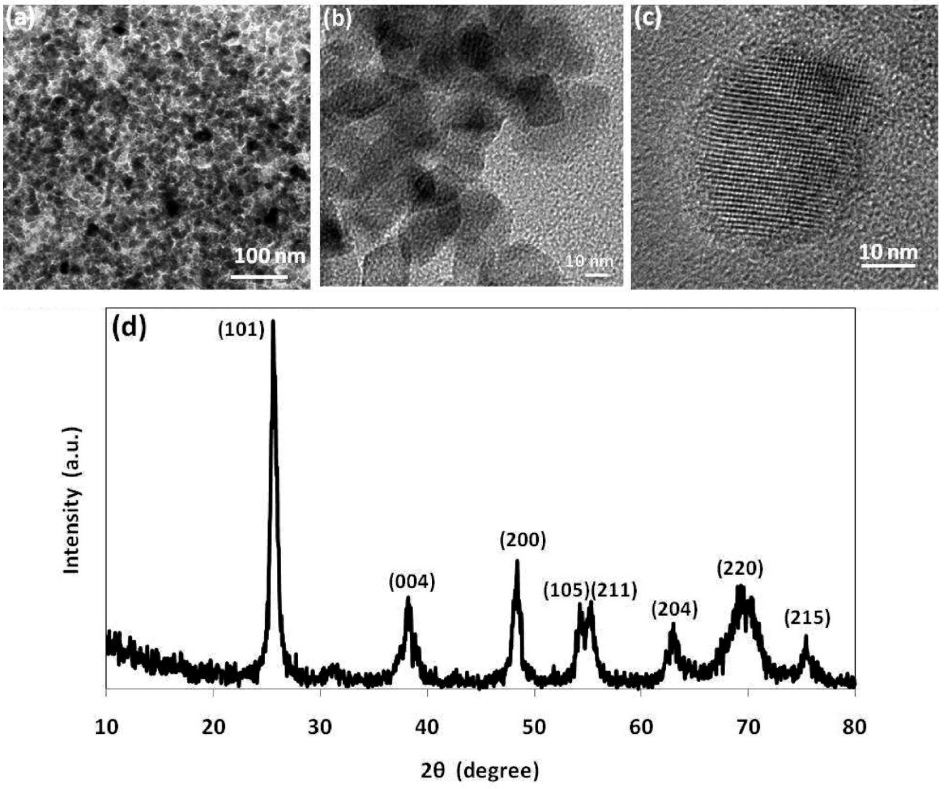

Figure 2. (a−c) TEM images and (d) XRD spectra of a TiO_2 nanoparticle film using 30 mL of titanium isopropoxide solution.

can be readily distinguished (Figure 2c). The TiO_2 nanoparticles have a size distribution of 20−40 nm. The pores observed in the image are presumably formed when the aggregation of the nanoparticles occurs during the calcination of the film. The corresponding wide-angle XRD pattern is shown in Figure 2d. The pattern shows several well-resolved peaks, which are indexed to the typical anatase phase of TiO_2. No other phase is detected in the synthesized films. It is already well established in the literature that anatase is the preferred phase for DSSC.[20−22] By analyzing the XRD peaks, the particle sizes of the TiO_2 sample can be calculated. The particle sizes are estimated using the Scherrer equation:[23]

$$t = \frac{(0.9\lambda)}{B\ cos\ \theta} \qquad (1)$$

where t is the particle size, λ the Cu $K\alpha$ wavelength, B the width of the peak at half the maximum intensity, and θ the diffracted angle at maximum intensity. The (101) peak is used to estimate the particle size. The estimated size of the TiO_2 nanoparticles is approximately 14 nm.

The nitrogen adsorption−desorption curve of the calcined nanoparticles is displayed in Figure 3a. The observed isotherm is type IV with a H2 type hysteresis loop. The nanoparticles (30 mL of titanium isopropoxide concentration) have relatively high BET surface area (~105 m^2g^{-1}) and a high pore volume (~0.3 ccg^{-1}), which are advantageous for dye adsorption. From the isotherms, it can be seen that the monolayer adsorption is not completed until reaching a relative pressure of 0.6, where the loop opens, indicating the existence of large pores. This is likely due to the formation of aggregated nanoparticles, which creates a porous film. A typical Gaussian type distribution of pore size,

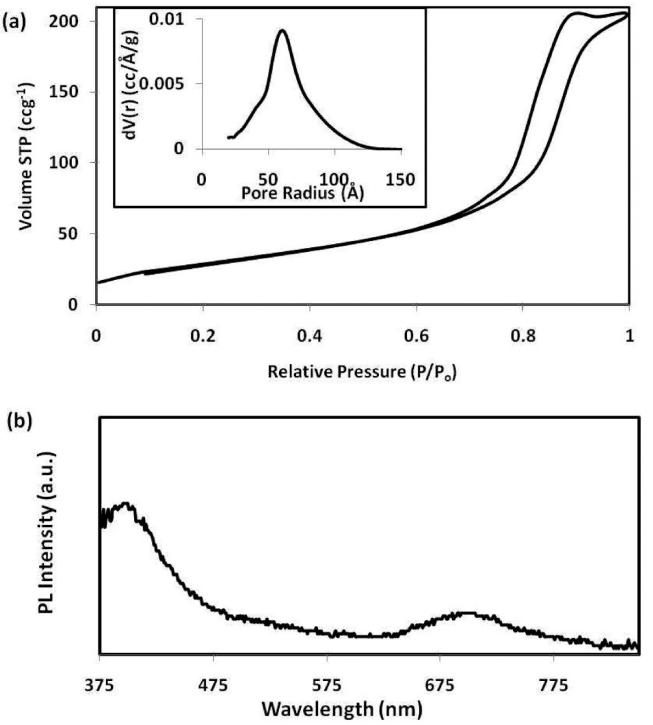

Figure 3. (a) Nitrogen adsorption−desorption isotherm at 77 K with the inset showing the corresponding pore size distribution and (b) photoluminescence spectrum for TiO_2 nanoparticles.

centered around 6 nm, is observed. BET surface area measurements for TiO_2 nanoparticles using a high concentration of

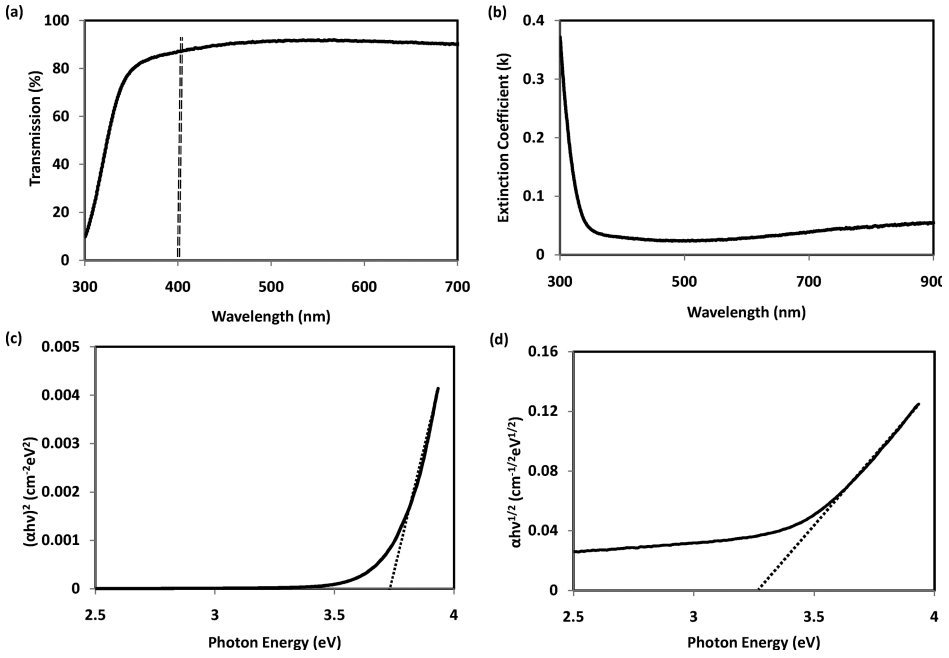

Figure 4. (a) Transmission spectrum, (b) computed extinction coefficient trend, (c) plot of $(\alpha h\nu)^2$ versus photon energy for direct transition, and (d) plot of $(\alpha h\nu)^{1/2}$ versus photon energy for indirect transition for TiO_2 nanoparticles.

titanium isopropoxide (60 mL) decreases (51 m^2g^{-1}) due to an increase in nanoparticle diameter and higher extent of agglomeration. The photoluminescence characteristic of the nanoparticles reveals broad bands (Figure 3b). The band gap energy of anatase TiO_2 is approximately 3.2 eV, which corresponds to a wavelength of 385 nm. The peak saturating at 390 nm is assigned to direct electronic transition from the conduction band to the valence band for the anatase structure and is in agreement with those reported in the literature.[24] The peak at 650−750 nm (centered around 700 nm) is attributed to the recombination of donors and acceptors trapped at interstitial TiO_2 sites.[25]

Transmittance studies are carried out using aqueous suspensions of the TiO_2 nanoparticles (Figure 4a). The film exhibits ∼80−85% transmittance in the UV and visible range (above 350 nm). The extinction coefficient (k) of the obtained data is calculated[26] and plotted in Figure 4b. It is observed that the value of k markedly decreases as wavelength increases in the range from 300 to 400 nm. The large magnitude of k (∼0.37) at 300 nm is attributed to the fundamental band gap and the low transmittance of film at short wavelengths. Band-to-band transition in the synthesized nanoparticles is also established by fitting the transmittance and absorption data (not shown) for direct and indirect band gap. The $(\alpha h\nu)^2$ versus photon energy plot for a direct transition (Figure 4c) and $(\alpha h\nu)^{1/2}$ versus photon energy plot for an indirect transition (Figure 4d) are displayed. Here, α is the absorption coefficient, and $h\nu$ is the photon energy. The value of photon energy extrapolated to α = 0 gives an absorption energy, which corresponds to the band gap E_g. For direct and indirect transition, the extrapolation yields E_g = 3.6 eV and E_g = 3.27 eV, respectively.

3.2. Characterization of Quasi-Solid-State Electrolytes. The DSSC, with the TiO_2 nanoparticle photoanode, is assembled using a quasi-solid-state electrolyte based on KI, LiI, and DPA. It is established in the literature that the conductivity of PEO-blended electrolytes increases with the size of the cation.[27] Since the ionic radius of K^+ ions (1.38 Å) is larger than Li^+ ions (0.76 Å),[28] it is expected that K^+ ions will have higher ionic conductivity. Thus, K^+ ions were added to the PEO electrolyte. Ionic conductivity, however, also depends on many other factors as seen from the following equation:

$$\sigma = n \cdot q \cdot \mu \tag{2}$$

where n is the density of charge carriers, q the number of electron charges per one carrier, and μ the mobility of the carriers. The density of charge carriers (n) is in turn related to the dissociation energy (U) and dielectric constant (ε):[29]

$$n = n_o exp\left[\frac{-U}{2\varepsilon K_B T}\right] \tag{3}$$

where K_B is the Boltzmann constant and T the absolute temperature. Hence, incorporating metal salts with higher mobility, higher dielectric constant, and lower dissociation energy can also enhance the ionic conductivity. From the above equations, it is clear that the ionic conductivity will be enhanced both by K^+ ions due to the larger ionic radius and by Li^+ ions due to the higher dielectric constant. Thus, both Li^+ and K^+ ions are incorporated in the electrolyte. K^+ ions are attracted to the ether oxygen of the PEO polymer,[30] thus acting as a filler to decrease the crystallization of the PEO polymer chain. DPA is added to increase the stability of the cell by reducing the sublimation of iodine in electrolytes. The nitrogen atom in DPA forms an interactive bond with I_2, which thus helps to reduce the sublimation of I_2 in the electrolyte.

One of the conditions for the electrolyte to be suitable for use in DSSC is that the light absorption by the electrolyte in the visible region should be as low as possible. This is to ensure that maximum light is absorbed by the N719 dye. N719 dye has an absorption maximum in the range of 350−550 nm with two prominent peaks around 380 and 530 nm. The absorption measurements of the quasi-solid electrolyte indicate that the absorption maximum occurs at the range of 350−400 nm. The UV−vis measurements were made on doctor bladed electrolyte

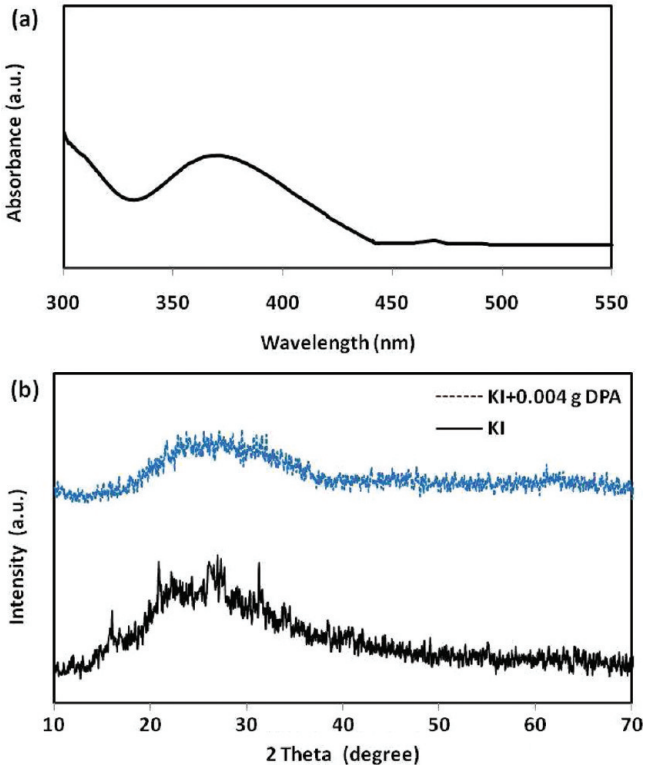

Figure 5. (a) Absorption spectrum for the 0.004 g DPA loaded electrolyte and (b) XRD spectra of PEO/KI/LiI based electrolyte with and without DPA loading.

Table 1. Photovoltaic Characteristics of DSSC at Various DPA Loadings in the Quasi-Solid-State Electrolyte

DPA concentration (wt %)	$V_{oc} \pm 0.002$ (V)	$J_{sc} \pm 0.1$ (mA cm^{-2})	FF ± 0.04 (%)	efficiency ± 0.03 (%)	R at V_{oc} ± 0.9 (Ω)
0.0	0.75	9.1	66.2	4.5	60.0
0.002	0.68	12.9	60.0	5.1	46.0
0.004	0.60	13.9	66.6	5.6	40.0
0.006	0.68	12.8	58.7	5.1	57.0
0.008	0.64	12.6	60.0	4.8	50.3
0.01	0.55	12.2	65.4	4.4	32.8

film on a glass slide. The broad maxima around 365 nm is due to $[I_3^-]$ and $[I^-]$.[31] The absorption spectrum of the DPA incorporated electrolyte overlaps with the N719 dye in the range of 380−400 nm, while the rest of the visible region has insignificant absorption. This weak absorption for wavelengths above 450 nm allows the use of highly concentrated electrolytes.

The XRD patterns of the KI incorporated PEO/LiI/I_2 quasi-solid electrolyte with and without DPA are shown (Figure 5b). Both electrolytes are mainly amorphous in nature, which is a clear indication that the KI ions effectively prevent the polymer PEO from crystallization. Since the intensity of the broad peak at approximately 25° decreased by ∼19%, we can infer that the amorphous nature of the electrolyte is slightly increased on addition of DPA. This also confirms the effective interaction between DPA and the polymer chain. The increased amorphous phase of PEO with DPA will favor inter- and intrachain ion movements and thus improve the electrical conduction.[32]

3.3. DSSC Performance Evaluation. Table 1 shows the photovoltaic behaviors of DSSC containing different amounts of DPA.

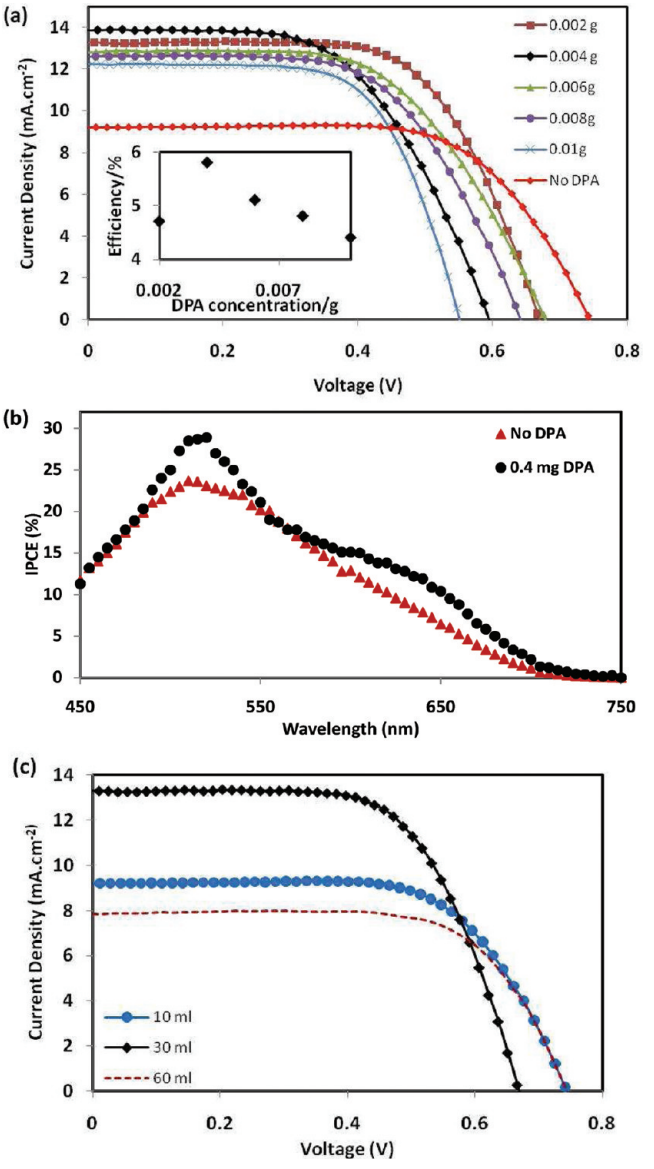

Figure 6. (a) J-V characteristics and (b) IPCE curves of DSSC employing a quasi-solid electrolyte with 0.0 and 0.0004 g of DPA. The inset shows the variation of the conversion efficiency with DPA loading. (c) J-V curve for DSSC with a photoanode made from 10, 30, and 60 mL of titanium isopropoxide solution.

It can be seen that the cell efficiency and J_{sc} increase on addition of a small quantity of DPA (Figure 6a). When the DPA is introduced into the KI filler polymer electrolyte, the cell efficiency increases from 4.5 to 4.7%. J_{sc} increases with increasing concentration of DPA up to 0.004 g, where a power conversion efficiency of 5.8% is achieved. J_{sc} decreases for DPA concentration greater than 0.004 g due to increased recombination in the device. Another reason may be that the higher concentration of DPA absorbs some of the visible light in the range of 350−420 nm, thus lowering the visible light absorption of the N719 dye. It is thus evident that there exists an optimum concentration of DPA below or above which the quasi-solid electrolyte loses its optimum performance. For iodine-based electrolytes, the decrease in I_3^- ion concentration is accompanied with an increase in I^- concentration.[33] The increase in the photocurrent values as more DPA is added into the electrolyte may be a

direct result of increased conductivity of the electrolyte. This could be a consequence of increased mobility of the redox species in the polymer electrolyte. The relatively high values of fill factor (*FF*) reflect low series resistance of the 0.004 g DPA electrolyte. For all other DSSC, the low *FF* may result from resistance losses arising from low ionic mobility of the redox species. The cell efficiencies at different DPA loadings in the KI polymer electrolyte are also displayed (inset Figure 6a). The enhanced device performance with DPA incorporated electrolyte can be explained by the interaction of highest occupied molecular orbital (HOMO) of donor DPA with lowest unoccupied molecular orbital (LUMO) of acceptor iodine. Higher stabilization energy can be achieved by reducing the energy difference between the HOMO of DPA and the LUMO of iodine, resulting in improved charge-transfer from donors to acceptors. The observed power conversion efficiencies of these cells are much higher than those reported using the pure polymer of the PEO/KI/I_2 system ($\sigma = 8.4 \times 10^{-5}$ Scm^{-1})[14] and polyethylene glycol systems using TiO_2 nanotubes ($\sigma = 2.4 \times 10^{-3}$ Scm^{-1}).[34]

IPCE is a powerful method to evaluate the light absorption, charge separation and transport, and charge collection in the DSSC device. The photocurrent action spectra of the DSSC employing the polymer electrolyte with and without DPA are shown (Figure 6b). Because of the UV cutoff effect caused by the glass substrate, the spectra under 400 nm are deteriorated. IPCE obtained for the DPA added electrolyte is higher than that without DPA in the wavelength region of 490−560 nm. An increased absorption in the visible light region for the range of 575−700 nm is also observed for the DPA added electrolyte. The evidence of the improvement in IPCE further confirms the higher J_{sc} achieved for the DPA incorporated electrolyte. The initial number of photogenerated carriers, electron injection efficiency, and the rate of recombination determine J_{sc} for the DSSC. Assuming the same injection efficiency and dye loading capacity of the TiO_2 nanoparticle films, it is reasonable to deduce that the increment in J_{sc} is due to the reduced recombination rate in the device.

The continuity equation, for DSSC by Lindquist,[35] describes the electron generation, diffusion, and interception as follows:

$$\frac{\partial n}{\partial t} = \eta_{inj} I_o \alpha e^{-ax} + Dn \frac{\partial^2 n}{\partial x^2} - \frac{n(x)}{\tau_n} = 0 \qquad (4)$$

It can be clearly seen that the absorption coefficient is directly proportional to the effective molar concentration of the dye, which is determined by the surface area and roughness of the nanomaterial framework. Hence, the effect of titanium isopropoxide concentration on the DSSC performance with the DPA (0.004 g) incorporated electrolyte is studied. The IV curves (Figure 6c) clearly reveal that for an electrode using 30 mL of titanium isopropoxide concentration (surface area ∼105 m^2g^{-1}), J_{sc} is the highest. However, 10 and 60 mL of titanium isopropoxide electrodes have lower J_{sc}. This is because these electrodes have irregular and agglomerated nanoparticles, which leads to lower surface areas of 85 and 51 m^2g^{-1}, respectively.

To further elucidate the photovoltaic performance of DSSC using 30 mL of titanium isopropoxide, EIS measurements are taken in the dark. The equivalent circuit that is used to model the impedance of the DSSC is shown (Figure 7a). The best devices using the PEO/KI/LiI/I_2 and PEO/KI/DPA/LiI/I_2 electrolyte system are used to study the effect of DPA addition in the electrolyte. The role of the electrolyte in DSSC is to facilitate the reduction of the photo-oxidized dyes. An effective electrolyte

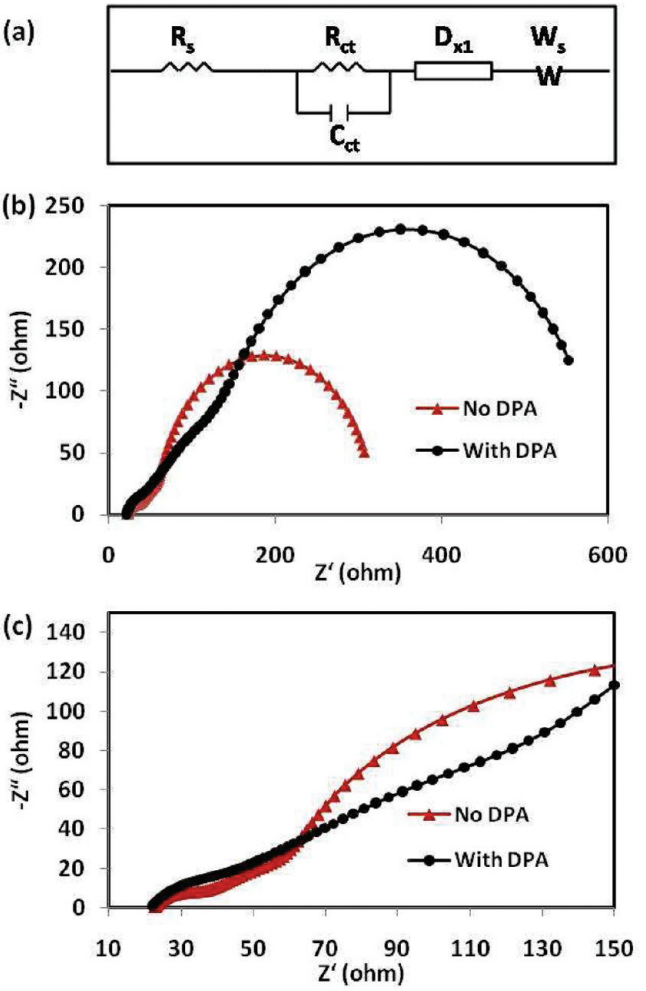

Figure 7. (a) Equivalent circuit model of the DSSC, (b) Nyquist plots, and (c) high resolution spectra in the high frequency region of the quasi-solid electrolyte DSSC.

should be capable of suppressing the recombination at the semiconductor−electrolyte interface, while promoting effective charge transport. The Nyquist plots for the DSSC device with and without the DPA electrolyte system are also shown (Figure 7b). Typically, there are three arcs in the impedance spectrum of a DSSC. The response at the high-frequency range (500000−1000 Hz) is attributed to the charge-transfer process at the electrolyte/Pt interface. The midfrequency range between 1000 and 1 Hz is governed by the charge-transfer process at the TiO_2/dye/electrolyte interface. It is generally assumed that these frequencies represent the recombination process between electrons in TiO_2 and the electrolyte. In the low-frequency region of 1−0.0002 Hz, the arc represents the mass transport resistance of ions in the electrolyte. A large semicircle at low frequencies for the DPA added electrolyte indicates an improved ion motion in the electrolyte. In the fit, the midfrequency arc is not distinguishable and sometimes missing in the spectra, indicating a small charge-transfer resistance at the TiO_2/dye/electrolyte interface. It may also happen that the charge-transfer at the TiO_2/dye/electrolyte interface is strongly dominated by the Pt/electrolyte interface. The fit results are presented in Table 2. The charge transport resistance (R_t) is lower for the DPA electrolyte DSSC, indicating that the introduction of DPA reduces the charge

Table 2. Impedance Spectra for DPA Free and 0.004 g of DPA Incorporated Electrolyte DSSC

device	R_t (Ω)	R_{ct} (Ω)	C_μ (μF)	τ_d (ms)	τ_n (ms)	D_n (cm^2s^{-1})	L_n (cm)	η_{cc}(%)	σ (Scm^{-1})
no DPA	3.0 ± 0.5	18.4 ± 0.5	470.0 ± 0.4	1.4 ± 0.20	8.6 ± 0.24	$2.9 \times 10^{-3} \pm 0.01$	5.0 ± 0.5	84.0 ± 0.1	$2.7 \times 10^{-3} \pm 0.001$
with DPA	2.4 ± 0.5	21.5 ± 0.5	360.0 ± 0.4	0.8 ± 0.18	8.0 ± 0.18	$4.5 \times 10^{-3} \pm 0.07$	6.0 ± 0.5	89.5 ± 0.2	$3.3 \times 10^{-3} \pm 0.001$

transport resistance at the interface of the Pt counter electrode and quasi-solid state electrolyte. At the same potential, the DPA incorporated electrolyte DSSC has a slightly larger charge-transfer (recombination) resistance (R_{ct}), which confirms the earlier claim of lower recombination rate in the DPA electrolyte. The difference in R_{ct} for both electrolytes at the electrolyte/Pt counter electrode interface is clearly visible in the high resolution scanned spectra of the high frequency region (Figure 7c). R_t is observed to be much smaller than R_{ct}, which is typically required for a high efficiency device.[36]

The electron transport or collection time (τ_d), time required for electrons to transport from the injection sites to the FTO, and the electron lifetime (τ_n) can be calculated as follows:[37]

$$\tau_d = R_t \cdot C_\mu \tag{5}$$

$$\tau_n = R_{ct} \cdot C_\mu \tag{6}$$

Here, C_μ is the chemical capacitance. It can be observed that the electrolyte with DPA has not only the longest lifetime but also a larger collection time. Since efficiency of the DSSC employing DPA incorporated electrolyte is higher, it can be inferred that although electron collection time is better for the electrolyte without DPA, its effect is compensated by the increased electron lifetime in the DPA added electrolyte. The effective diffusion length (L_n) of electrons in the TiO_2 film is yet another critical parameter that affects the charge collection efficiency. It can be calculated as follows:[37]

$$L_n = \sqrt{D_n \tau_n} = L\sqrt{\frac{\tau_n}{\tau_d}} \tag{7}$$

As can been seen from Table 2, L_n increases as the DPA is added in to the PEO/KI/LiI/I_2 electrolyte. L_n is much larger than the TiO_2 thickness for both the electrolytes, which indicates good collection efficiency. The increase in L_n may be caused by suppression of the recombination rate in the DPA electrolyte, as already seen.

The conductivity of the electrolytes (σ) is derived from the complex impedance measurements using the following equation:

$$\sigma = \frac{L}{AR_b} \tag{8}$$

where R_b is the bulk resistance determined from the intersection of the high-frequency semicircle with the real axis, L is the thickness of the film, and A is the area of the sample. An increment of ~30% is achieved in conductivity when DPA is added in the filler free PEO/KI/LiI/I_2 electrolyte system. It is important to note that this increase in ionic conductivity is achieved without compromising the mechanical strength of the electrolyte, as no inorganic filler is added.

The fitted values of R_t, R_{ct}, and C_μ at bias values of 0.65 and 0.7 V are shown (Figure 8). The dependence of R_{ct} on the applied forward bias[38] can be expressed as follows:

$$R_{ct} = R_o exp\left(-\beta \frac{qV}{K_B T}\right) \tag{9}$$

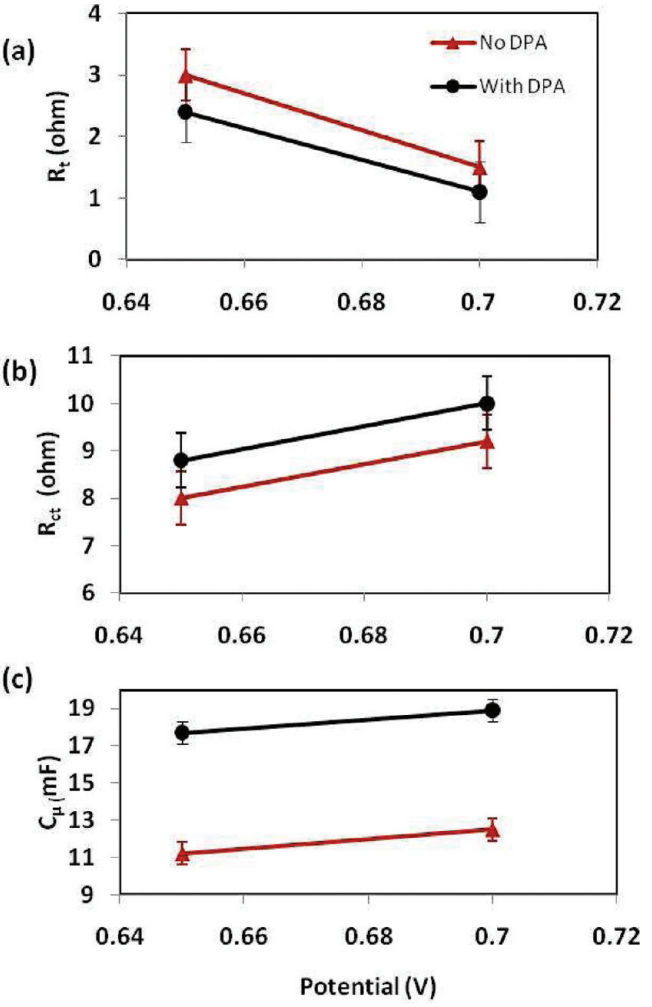

Figure 8. Forward bias dependence of (a) transport resistance (R_t), (b) charge-transfer (recombination) resistance (R_{ct}), and (c) chemical capacitance (C_μ) of the quasi-solid electrolyte DSSC.

where R_o is a constant, β the transfer coefficient, q the elemental charge, K_B the Boltzmann constant, and T the temperature. The plot demonstrates a much stronger forward bias dependence for the electrolyte without DPA. It is known that once the electrons transport along the TiO_2 surface, the surface traps will enhance R_t and reduce σ. When DPA is added to the electrolyte, the trap related recombination may be suppressed, which reduces R_t and increases σ. The reduction in R_t is consistent with increased R_{ct} at the TiO_2/electrolyte interface. The C_μ increases with the applied potential in both electrolytes, indicating a high charge accumulation and effective electrical communication between the Fermi level in TiO_2 and FTO. The C_μ can be estimated as follows:[39]

$$C_\mu = C_o exp\left[-\alpha \frac{qV}{K_B T}\right] \tag{10}$$

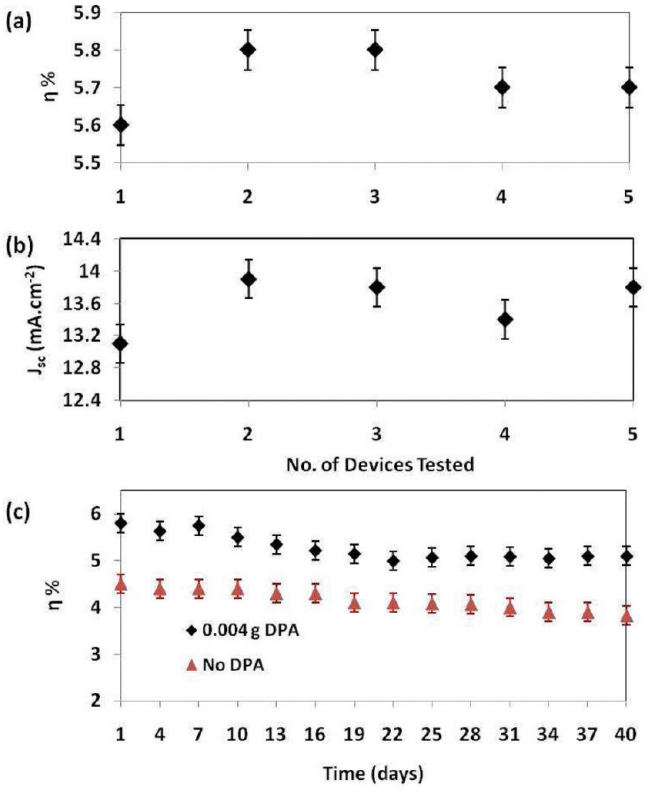

Figure 9. (a) DSSC performance of five devices tested for reproducibility. (b) Stability for the quasi-solid state DSSC.

where C_o is a constant, and $\alpha = T/T_o$; T_o being the characteristic temperature indicating the depth of the distribution. From this discussion, it is clear that the only disadvantage of adding DPA in the electrolyte seems to be lower V_{oc} for the device. V_{oc} is mainly influenced by the rate of recombination in DSSC and the shift in the conduction band edge (E_c) of the metal oxide semiconductor. Li^+ cations are known to shift the E_c of TiO_2 downward.[40] It is suspected that the DPA incorporated electrolyte shifts the E_c by a large quantity, which leads to lower V_{oc}. The suppressed interfacial charge recombination and better electron lifetime, however, compensate the adverse effect of band edge movement on V_{oc}. Hence, the net effect is increased conversion efficiency of the DSSC employing DPA added electrolyte.

In order to ascertain the reproducibility of the devices, five different devices from different batches of materials are made and tested. The trend of η and J_{sc} is recorded for the tested devices (Figure 9a). One of the motivations for the substituting liquid electrolyte with the quasi-solid electrolyte is to minimize leakage and solvent evaporation; ensuring longer stability and longer life for the DSSC. Thus, studying the stability of DSSC with the DPA incorporated quasi-solid state electrolyte is also important. An evaluation of the efficiency during the aging period for DSSC assembled with PEO/KI/DPA/LiI/I_2 electrolyte system is given (Figure 9b). An initial decay in efficiency is reported which is followed by a slight increase. The increase in efficiency could be attributed to better wetting of the TiO_2 nanoparticle film by the electrolyte through improved seepage of the electrolyte. The efficiency, however, continues to decrease after a week but eventually stabilizes after 25 days. It has been suggested that the initial decay in the performance followed by a plateau of stability might be an intrinsic property of DSSC assembled with polymer electrolytes. This trend is independent of the cell size, substrate type, and exposure time.[41] Since deposition of the quasi-solid electrolyte takes place under heating, no residue solvent is left behind. Therefore, the loss of performance for the DSSC cannot be attributed to the evaporation of the solvent. The loss of power conversion efficiency over time may come from degradation of the N719 dye. It is well understood that the regeneration of the dye in DSSC is a very fast process. Under the lack of favorable conditions, however, the dye may remain in oxidized state for long periods leading to degradation through the loss of the −NCS ligand.[42] This is especially true for the quasi-solid state DSSC because the ion mobility is low in the electrolyte. This can lead to slow regeneration or incomplete filling of TiO_2 nanoparticles by the electrolyte. Hence, degradation of the DSSC device may be due to a number of reasons which may not be independent of each other. Desorption of the dye, degradation of the counter electrode, and changes in electron transport in the semiconductor are some of them. The DPA added quasi-solid DSSC loses only 11% of the initial performance. The stability figures are very impressive compared to those of the liquid electrolyte DSSC, which loses almost half the conversion efficiency after 5 days. It is also note worthy that this stability is achieved without adding any plasticizer or inorganic filler, which might compromise the mechanical strength of the electrolyte. The stability results of the DPA incorporated quasi-solid electrolyte ascertain the benefits of replacing the liquid component.

4. CONCLUSIONS

This work investigates the influence of titanium isopropoxide dosage on the morphology of TiO_2 nanoparticles. Anatase phase nanoparticles with a diameter of 15−20 nm and a surface area of ∼105 m^2g^{-1} are synthesized and used to fabricate the working electrode with the implementation of a filler free DPA electrolyte. In the electrolyte, KI acts as a filler to reduce the crystallinity of the PEO matrix, and DPA reduces the sublimation of I_2. DSSC employing this electrolyte shows a conversion efficiency of 5.8%, which is attributed to enhanced ionic conductivity (∼3.5×10^{-3} Scm^{-1}). EIS results indicate suppressed interfacial charge recombination and better electron lifetime with the addition of DPA. The device is stable and retains 89% of the initial efficiency after 40 days.

AUTHOR INFORMATION

Corresponding Author

*Engineering Science, EA 07-37, Blk E3A #04-17, National University of Singapore, Singapore 11757474. Phone: (65) 6516 8121. E-mail: elehgw@nus.edu.sg.

ACKNOWLEDGMENT

This work was supported by the National University of Singapore and Applied Materials. We thank Mr. Andrew See Weng Wong and Chee Hong Chua for their contributions.

REFERENCES

(1) Bach, U.; Lupo, D.; Comte, P.; Moser, J. E.; Weissörtel, F.; Salbeck, J.; Speritzer, H.; Grätzel, M. *Nature (London)* **1998**, *395*, 583–585.

(2) Fukuri, N; Masaki, N.; Kitamura, T.; Wada, Y.; Yanagida, S. *J. Phys.Chem. B* **2006**, *110*, 25251–25258.

(3) Meng, Q. B.; Takahashi, K.; Zhang, X. T.; Sutanto, I.; Rao, T. N.; ato, O.; Fujishima, A. *Langmuir* **2003**, *19*, 3572–3574.

(4) O'Regan, B.; Lenzmann, F.; Muis, R.; Wienke, J. *Chem. Mater.* **2002**, *14*, 5023–5029.
(5) Dai, Q.; MacFarlane, D. R.; Howlett, P. C.; Forsyth, M. *Angew. Chem., Int. Ed.* **2005**, *44*, 313–316.
(6) Nogueira, A. F.; Longo, C.; De Paoli, M.-A. *Coord. Chem. Rev.* **2004**, *248*, 1455–1468.
(7) Nogueira, A. F.; Durrant, J. R.; De Paoli, M.-A. *Adv. Mater.* **2001**, *13*, 826–830.
(8) Kim, J. H.; Kang, M.-S.; Kim, Y. J.; Won, J.; Kang, Y. S. *Solid State Ionics* **2005**, *176*, 579–584.
(9) Kubo, W.; Murakoshi, K.; Kitamura, T.; Yoshida, S.; Hakuri, M.; Hanabusa, K.; Shirai, H.; Wada, Y.; Yanagida, S. *J. Phys. Chem B* **2001**, *105*, 12809–12815.
(10) Kang, J.; Li, W.; Wang, X.; Lin, Y.; Li, X.; Xiao, X.; Fang, S. *J. Appl. Electrochem.* **2004**, *34*, 301–304.
(11) Wang, P.; Zakeeruddin, S. M.; Moser, J.-E.; Balker, R. H.; Grätzel, M. *J. Am. Chem. Soc.* **2004**, *126*, 7164–7165.
(12) Matsumoto, H.; Matsuda, T.; Tsuda, T.; Hagiwara, R.; Ito, Y.; Miyazaki, Y. *Chem. Lett.* **2001**, *30*, 26–27.
(13) Ren, Y. J.; Zhang, Z. C.; Fang, S. B.; Yang, M. Z.; Cai, S. M. *Sol. Energy Mater. Sol. Cells* **2002**, *71*, 253–259.
(14) Kalaignam, G. P.; Kang, M. S.; Kang, Y. S. *Solid State Ionics* **2006**, *177*, 1091–1097.
(15) Matsui, H.; Okada, K.; Kitamura, T.; Tanabe, N. *Sol. Energy Mater. Sol. Cells* **2009**, *93*, 1110–1115.
(16) Gorlov, M.; Kloo, L. *Dalton Trans.* **2008**, *20*, 2655–2666.
(17) Muthuraaman, B.; Murugesan, S.; Mathew, V.; Ganesan, S.; Paul, B. J.; Madhavan, J.; Maruthamuthu, P.; Suthanthiraraj, S. A. *Sol. Energy Mater. Sol. Cells* **2008**, *92*, 1712–1717.
(18) Ganesan, S.; Muthuraaman, B.; Mathew, V.; Madhavan, J.; Maruthamuthu, P.; Suthanthiraraj, S. A. *Sol. Energy Mater. Sol. Cells* **2008**, *92*, 1718–1722.
(19) Ding, I.-K.; Melas-Kyriazi, J.; Cevey-Ha, N.-L.; Chittibabu, K. G.; Zakerruddin, S. M.; Grätzel, M.; McGehee, M. D. *Org. Elect.* **2010**, *11*, 1217–1222.
(20) Park, N. G.; Van de Lagemaat, J.; Frank, A. J. *J. Phys. Chem. B* **2000**, *104*, 8989–8994.
(21) Kalyanasundaram, K.; Grätzel, M. *Coord. Chem. Rev.* **1998**, *177*, 347–414.
(22) Agarwala, S.; Kevin, M.; Wong, A. S. W.; Peh, C. K. N.; Thavasi, V.; Ho, G. W. *ACS Appl. Mater. Interface* **2010**, *2*, 1844–1850.
(23) Cullity, B. D. *Elements of X-Ray Diffraction*, 2nd ed.; Addison-Wesley Publishing Company, Inc.: Boston, MA, 1956; p 86.
(24) Zhang, W. F.; Zhang, M. S.; Yin, Z.; Chen, Q. *Appl. Phys. B: Laser Opt.* **2000**, *70*, 261–265.
(25) Poznyak, S. K.; Sviridov, V. V.; Kulak, A. I.; Samtsov, M. P. *J. Electroanal. Chem.* **1992**, *340*, 73–97.
(26) Hong, W. Q. *J. Phys. D: Appl. Phys.* **1989**, *22*, 1384–1385.
(27) Bhattacharya, B.; Lee, J. Y.; Geng, J.; Jung, H.-T.; Park, J.-K. *Langmuir* **2009**, *25*, 3276–3281.
(28) Dean, J. A. *Lange's Handbook of Chemistry*, 14th ed.; Mc Graw-Hill: New York, 1992.
(29) Barker, R. E.; Thomas, C. R. *J. Appl. Phys.* **1964**, *35*, 3203–3215.
(30) De Freitas, J. N.; Nogueira, V. C.; Ito, B. I.; Soto-Oviedo, M. A.; Longo, C.; De Paoli, M.-A.; Nogueira, A. F. *Int. J. Photoenergy* **2006**, *75483*, 1–6.
(31) Kebede, Z.; Lindquist, S. E. *Sol. Energy Mater. Sol. Cells* **1999**, *57*, 259–275.
(32) Preechatiwong, W.; Schultz, J. M. *Polymer* **1996**, *37*, 5109–5116.
(33) Kusama, H.; Arakawa, H. *Sol. Energy Mater. Sol. Cells* **2004**, *81*, 87–99.
(34) Akhtar, M. S.; Chun, J. M.; Yang, O.-B. *Electrochem. Commun.* **2007**, *9*, 2833–2837.
(35) Sodergren, S.; Hagfeldt, A.; Olsson, J.; Lindquist, S. E. *J. Phys. Chem.* **1994**, *98*, 5552–5556.
(36) Martinson, A. B. F.; Goes, M. S.; Fabregat-Santiago, F.; Bisquert, J.; Pellin, M. J.; Hupp, J. T. *J. Phys. Chem. A* **2009**, *113*, 4015–4021.
(37) Bisquert, J.; Fabregat-Santiago, F.; Mora-Seró, I.; Garcia-Belmonte, G.; Giménez, S. *J. Phys. Chem. C* **2009**, *113*, 17278–17290.
(38) He, C.; Zheng, Z.; Tang, H.; Zhao, L.; Lu, F. *J. Phys. Chem. C* **2009**, *113*, 10322–10325.
(39) Xie, Y.; Prakash, J.; Darling, S. B.; Chen, Q.; Zhang, T.; Galipeau, D.; Qiao, Q. *J. Phys. Chem C* **2010**, *114*, 17880–17888.
(40) Qu, P.; Meyer, G. J. *Langmuir* **2001**, *17*, 6720–6728.
(41) De Freitas, J. N.; Nogueira, A. F.; De Paoli, M. A. *J. Mater. Chem.* **2009**, *19*, 5279–5294.
(42) Grünwald, R.; Tributsh, H. *J. Phys. Chem. B* **1997**, *101*, 2564–2575.